Light acclimation interacts with thylakoid ion transport to govern the dynamics of photosynthesis

Thekla von Bismarck
Max Planck Institute of Molecular Plant Physiology https://orcid.org/0000-0002-8523-5313
Kübra Korkmaz
Max Planck Institute of Molecular Plant Physiology
Jeremy Ruß
Max Planck Institute of Molecular Plant Physiology
Kira Skurk
Max Planck Institute of Molecular Plant Physiology
Elias Kaiser
Wageningen University and Research
Viviana Correa Galvis
Max Planck Institute of Molecular Plant Physiology
Jeff Cruz
Michigan State University
Deserah Strand
Max Planck Institute of Molecular Plant Physiology
Karin Köhl
Max Planck Institute of Molecular Plant Physiology
Jürgen Eirich
University of Münster https://orcid.org/0000-0003-0963-1872
Iris Finkemeier
Institut für Biologie und Biotechnologie der Pflanzen, Schlossplatz 7 ,48149 Muenster, Germany
Peter Jahns
Heinrich Heine University Düsseldorf
David Kramer
Michigan State University https://orcid.org/0000-0003-2181-6888
Ute Armbruster (armbruster@mpimp-golm.mpg.de)
Max Planck Institute of Molecular Plant Physiology https://orcid.org/0000-0002-8814-8207

Article

Keywords: photosynthesis, light acclimation, light-environment

Posted Date: September 29th, 2021

DOI: https://doi.org/10.21203/rs.3.rs-948381/v1

Light acclimation interacts with thylakoid ion transport to govern the dynamics of photosynthesis

Thekla von Bismarck[1], Kübra Korkmaz[1], Jeremy Ruß[1], Kira Skurk[1], Elias Kaiser[1, §], Viviana Correa Galvis[1, #], Jeffrey A. Cruz[2, 3], Deserah D. Strand[1, %], Karin Köhl[1], Jürgen Eirich[4], Iris Finkemeier[4], Peter Jahns[5], David M. Kramer[2, 3] and Ute Armbruster[1*]

[1]Max Planck Institute of Molecular Plant Physiology, Potsdam, Germany

[2]DOE-Plant Research Laboratory, Michigan State University, East Lansing, Michigan, USA

[3]Department of Biochemistry and Molecular Biology, Michigan State University, East Lansing, Michigan, USA

[4]Plant Physiology, Institute of Plant Biology and Biotechnology, University of Münster, Münster Germany

[5]Plant Biochemistry, Heinrich-Heine-University Düsseldorf, Düsseldorf, Germany

*Corresponding author e-mail: armbruster@mpimp-golm.mpg.de

Current addresses:

§ Horticulture and Product Physiology, Department of Plant Sciences, Wageningen University, Wageningen, the Netherlands

InFarm – Indoor Urban Farming GmbH, Berlin, Germany

% DOE-Plant Research Laboratory, Michigan State University, East Lansing, Michigan, USA State University, East Lansing, Michigan

Abstract:

Understanding photosynthesis in natural, dynamic light environments requires knowledge of long-term acclimation, short-term responses, and their mechanistic interactions. However, the latter is poorly understood. We systematically determined light-environment effects on the thylakoid ion transport-mediated responses of photosynthesis during light fluctuations. Our analyses reveal daily light intensity as the main acclimatory driver that sculps photosynthetic capacity and thereby governs the activities of the thylakoid Cl^- channel VCCN1 and the H^+/K^+ exchanger KEA3 during high light phases. We uncover high zeaxanthin accumulation as a response to fluctuating light environments, which delays the relaxation of energy dependent quenching (qE). KEA3 partly suppresses zeaxanthin accumulation over the day and thereby further accelerates the response of photosynthesis to low light periods. In summary, both light-environment factors, intensity and variability, modulate the function of thylakoid ion transport in dynamic photosynthesis with distinct effects on lumen pH, zeaxanthin accumulation, qE and photosynthetic light use efficiency.

Plant photosynthesis uses available light for biomass production. In crop field canopies, light intensity fluctuates immensely[1]. Due to the relative evolutionary recency of dense crop canopies, photosynthesis may not be fully optimized for strong fluctuations in light intensity. A detailed understanding of dynamic photosynthesis is needed to identify mechanistic shortcomings and successfully manipulate photosynthesis for increased biomass in the field.

Mechanistic understanding is required on two time-scales: long-term acclimation to natural dynamic light environments, and short-term responses to changes in light intensity. For the model plant *Arabidopsis thaliana* (Arabidopsis), it has been shown that light acclimation involves the upregulation of photosynthetic capacity with light intensity[2-11] and natural environment acclimation increases photoprotective capacity[8,9,12]. Only a small number of short-term regulatory factors has been characterized under natural field conditions[13-15], leaving a knowledge gap between physiological functions determined in the lab and in nature.

The dissipation of absorbed light energy as heat, termed non-photochemical quenching (NPQ), is required for plant fitness in the field[14]. Energy dependent NPQ (qE), the main and most rapid NPQ component in plants[16], involves the PsbS protein, photosystem (PS) II supercomplex rearrangements triggered by PsbS, and zeaxanthin[17]. qE is proportional to the proton concentration of the lumen[18-21], and the PsbS protein as well as zeaxanthin (Zx) synthesis from violaxanthin by the violaxanthin-deepoxidase (VDE) are activated upon protonation of key amino acid residues[19,22]. Whether zeaxanthin is involved in the dissipation of light energy itself or affects qE dynamics is under discussion[23-27].

The light reactions in the thylakoid membrane lead to an accumulation of protons in the lumen, forming the proton motive force (pmf), which is composed of a membrane potential ($\Delta\psi$) and the proton concentration gradient (ΔpH), driving ATP synthesis via the ATP synthase[28]. When absorbed light energy exceeds the capacity of downstream metabolic reactions, the rate of proton influx into the lumen becomes higher than efflux via the ATP synthase, leading to onset of qE. For an imbalance in proton fluxes to incur changes in the lumenal proton concentration and thus qE, some $\Delta\psi$ needs to be dissipated[29]. The high $\Delta\psi$-activated Cl^- channel VCCN1 participates in lowering $\Delta\psi$ and thereby accelerates qE induction in excess light[13,30]. Conversely, the thylakoid localized K^+/H^+ exchanger KEA3 activates after transition to photosynthesis-limiting light intensities, lowers the lumenal proton concentration, thereby re-establishing some $\Delta\psi$, accelerating qE relaxation and increasing photosynthetic light use efficiency[31,32]. Under excess light, KEA3 inactivates via its C-terminus[32,33],

sustaining high levels of qE and protecting the photosystems from photodamage[33]. Both thylakoid ion transport proteins, VCCN1 and KEA3, shape dynamic photosynthesis by controlling the lumenal proton concentration and therefore the photosynthetic response during light fluctuations.

The present study addresses how long-term acclimation to different light intensities and patterns affects photosynthetic responses to changes in light intensity. We distinguished effects of two light-environmental drivers and analyzed interactions with the known thylakoid ion transport proteins KEA3 and VCCN1, by using a modified non-invasive spectroscopy method for monitoring ion flux dynamics at unprecedented high temporal resolution *in planta*.

Results:

Growth light intensity is the main determinant of steady-state photosynthesis.

To bridge the gap between experimental and natural light environments, different average photon flux densities (PFD_{mean}) and intensity variations (quantified as sum of all light intensity changes over the day, PFD_{var}) were combined in six treatments of Arabidopsis wild-type (WT) plants under controlled phytotron conditions (Fig. 1a, Supplemental Fig. 1a-f): flat day with low (FD_L), medium (FD_M) or high (FD_H) light intensities, dynamic day with step-wise light fluctuations (DD_F), sinusoidal day alone (DD_S) or together with random fluctuations (DD_{SF}) with. Additionally, plants were grown under natural light and climate in a polytunnel (natural day, ND_1 and ND_2; Fig. 1b, Supplemental Fig. 1g-i, Supplemental Table_Fig1a-b_SFig1). Multiple regression analysis revealed PFD_{mean} as the predominant factor that could explain differences observed in steady-state photoprotection (NPQ) and PSII quantum efficiency (Φ_{PSII}) during a light-response curve, with a minor role of PFD_{var} (Supplemental Fig. 2a-b, Supplemental Results, Supplemental Table_SFig2a-b). Φ_{PSII} measured at high irradiance linearly increased with and saturated at high PFD_{mean} (Fig. 1c). PFD_{mean} was also the main factor explaining differences in gross carbon assimilation rates (A_g) at high irradiance between conditions (Fig. 1d, Supplemental Results, Supplemental Table_Fig1d_SFig2c). A_g showed a very similar dependency on PFD_{mean} as Φ_{PSII}, except for natural environment-grown ND, which had decreased values of A_g per PFD_{mean} compared to phytotron-grown plants (Fig. 1d). One possible explanation for this discrepancy between Φ_{PSII} and CO_2 assimilation seen in ND are higher rates of electron transport from PSII to alternative acceptors, as a consequence of natural environment acclimation.

Fluctuating light boosts levels of photoprotective xanthophylls.

To obtain insight into light environmental effects on the composition of the photosynthetic apparatus (Supplemental Fig. 4a), we determined pigment and protein contents. The levels of the light harvesting complex of PSII (LHCII) correlated negatively and PSII positively with PFD_{mean} (Supplemental Fig. 4b). A PFD_{mean}-dependent increase in reaction center per antenna ratio was supported by levels of reaction center-bound ß-carotene and the Chl *a*/*b* ratio rising with PFD_{mean} (Supplemental Fig. 4c). Levels of Cyt b_6f complex and chloroplast ATP synthase correlated positively, and LHCII and PSI negatively with PFD_{var} (Supplemental Fig. 4b). The violaxanthin-antheraxanthin-zeaxanthin (VAZ) pool size as well as its de-epoxidation state (DEPS) were predominantly shaped by PFD_{var} as the main factor (Fig. 1e-f, Supplemental Table_Fig1e-f). This was especially pronounced for DEPS, which was more than twofold increased in plants grown under strongly fluctuating light compared to the other conditions.

Thylakoid ion transport shapes dynamic NPQ in a light-environment dependent manner.

To assess the effect of light acclimation on NPQ during fluctuations in light intensity, we exposed plants to alternating low and high irradiances (LI and HI, respectively) and found most of the characterized NPQ parameters to correlate negatively with PFD_{mean} (Supplemental Fig. 5a-f). This finding agreed with the results from steady-state photosynthesis, which showed that acclimation to high PFD_{mean} reduced levels of NPQ (Supplemental Fig. 2a). Interestingly, ND plants showed higher NPQ induction during HI phases as compared to the other conditions, apparently suppressing the accumulation of slowly relaxing NPQ components (Supplemental Fig. 5g-h).

To determine the effects of environmental acclimation on the function of VCCN1 as a facilitator, and KEA3 as an inhibitor of lumenal acidification and thus qE, we evaluated NPQ of two mutant alleles each of *KEA3* and *VCCN1* during light fluctuations (Fig. 2a-b; Supplemental Fig. 6). Mutants grown under the various light conditions visually resembled the respective WT and showed comparable maximum PSII quantum efficiency (Fv/Fm; Supplemental Fig. 7a-i). Mutant NPQ values during the third fluctuation, the final LI measuring point and after 5 min in the dark (Fig. 2a) were compared with WT (Fig. 2c). NPQ of both mutants, *vccn1* and *kea3*, differed strongly from WT with lower and higher values of *vccn1* and *kea3*, respectively, under HI and strongly increased NPQ levels in *kea3* during relaxation in LI (Fig. 2c). K-mean clustering of log_2 transformed mutant/WT NPQ ratios defined two separate groups, of which one contained only *vccn1* and the other mainly *kea3*. Multiple regression analysis

revealed significant effects of PFD_{mean} and PFD_{var} on the function of the two thylakoid ion transport proteins during light fluctuations (Supplemental Table_Fig2c_SFig8). Most interestingly, PFD_{mean} had opposing effects on *vccn1* and *kea3* phenotypes during the HI phase: while the low NPQ phenotype of *vccn1* decreased and NPQ became more similar to WT, the high NPQ phenotype of *kea3* increased with PFD_{mean} (Supplemental Fig. 8a-b). After 30 s in HI, the linear NPQ phenotype correlation with PFD_{mean} was stronger for *vccn1* than *kea3* (ρ = 0.56 and 0.36, respectively), while after 1 min HI the reverse was observed (ρ = 0.34 and 0.92, respectively). These results suggest a sequential activation and function of the two proteins during high light phases, which respond oppositely to PDF_{mean}. Additionally, PFD_{var} as the second light factor, significantly enhanced the high NPQ phenotype of *kea3* mutants specifically during relaxation at LI.

Growth light intensity determines impact of thylakoid ion transport on photosynthetic efficiency.

To examine the impact that observed alterations in NPQ dynamics had on photosynthetic efficiency, we analyzed the relationship between NPQ and PSII quantum yield. 30 s after transition from LI to HI, the overall inverse Φ_{PSII}-NPQ correlation was relatively weak (ρ = -0.50, Fig. 3a). Stronger negative correlations became evident when each growth condition was examined separately (Supplemental Table_Fig3_SFig9). The slopes of the condition-specific Φ_{PSII}-NPQ relationships were found to correlate strongly with PFD_{mean}, particularly when ND was excluded (Fig. 3a, lower panel). After 1 min HI, the overall correlation increased (ρ_{all} = -0.73; Supplemental Fig. 9a). During NPQ relaxation in LI, Φ_{PSII} correlated near-linearly with NPQ, independently of environmental factors, with *kea3* mutants from most growth conditions (except for high PFD_{mean}) forming a separate group with higher NPQ and lower Φ_{PSII} compared to the other genotypes (Fig. 3b, Supplemental Fig. 9b). The data uncover that thylakoid ion transport-mediated changes in NPQ affect photosynthetic efficiency particularly during HI-induction and under environmental conditions with high PFD_{mean}.

An additional set of experiments exposed plants from three selected environments, with strongly differing effects on thylakoid ion transport mutant phenotypes (i.e., FD_L: low PFD_{mean}; FD_H: high PFD_{mean} and DD_F: intermediate PFD_{mean}, high PFD_{var}), to increasing durations of HI (Supplemental Fig. 10-11). These analyses revealed that the Φ_{PSII}-NPQ correlations of the mutants from the separate environments became weaker with increasing durations of HI (Supplemental Fig. 11m-n, Supplemental Table_SFig11). After 10 min HI, Φ_{PSII} of *kea3* mutants did no longer correlate with NPQ, but was instead

determined by growth conditions and very similar to those of the other two genotypes, with net CO_2 assimilation rate (A_n) of all genotypes strongly correlating with Φ_{PSII} (Supplemental Fig. 11o-p, Supplemental Table_SFig11). As a consequence, FD_H-grown *kea3* showed no and DD_F-grown *kea3* only slight decreases in A_n at HI compared to WT, despite having strongly elevated NPQ (Supplemental Fig. 11h-i, k-l). No significant effects of *kea3* or *vccn1* on biomass were observed under any condition (Supplemental Fig. 12).

Light acclimation alters the activation of VCCN1 and KEA3 during light fluctuations.

The three selected environments were further employed to delineate light acclimation effects on VCCN1 and KEA3 activation and function at milliseconds time resolution. For this, we near-simultaneously measured shifts in the absorption spectra of qE (a proxy for lumenal proton concentration), and the electrochromic shift (ECS) around 520 nm, which reports on the membrane potential (Δψ, Fig 4a). The same short fluctuating light regime was applied as before (Fig. 2a) with an additional dark phase 20 s after the shift to LI, to follow the multiphasic decay of the ECS signal, allowing the estimation of ∆pH and ∆ψ contribution to pmf composition[34,35]. No differences in pigment composition between genotypes were observed for a given light environment, permitting the direct comparison of absorption signals between WT and mutants (Supplemental Table_Fig4).

In general, growth light conditions strongly affected the responses of both, qE and ∆ψ, to the fluctuating light regime (Fig. 4b,c). Loss of either VCCN1 or KEA3 further influenced these responses in an environment-dependent manner. After transition from LI to HI, induction of NPQ and qE always showed a distinct lag phase in *vccn1* (Fig. 4b, Supplemental Fig. 13). This lag was particularly pronounced in FD_L grown plants, in which it was accompanied by increased Δψ throughout the entire HI-phase (Fig. 4c). For the other two light environments (i.e. FD_H and DD_F), Δψ did not differ markedly between *vccn1* and WT. During the HI phase, no NPQ or qE differences were observed between *kea3* and WT from FD_L, while qE of *kea3* was increased both in FD_H and DD_F, supporting that in contrast to FD_L, KEA3 is activated to suppress HI-qE under these two conditions (Fig. 4b, Supplemental Fig. 13). In FD_H, HI-qE relaxed in WT after ~15 s, but remained at the same high level in *kea3*. The *kea3* mutants from DD_F and FD_H showed reduced levels of Δψ at 6 and 8 s, respectively, after shift from LI to HI (Fig. 4c), at which time point Δψ strongly increased in WT particularly from FD_H. After transition back to LI, WT had accelerated qE relaxation when compared to *kea3*, most pronouncedly in FD_L and DD_F (Fig. 4b), which

was accompanied by a stronger increase and higher levels of Δψ in WT as compared to *kea3* following an initial steep dip (Fig. 4c).

These time-resolved measurements of qE and Δψ during the HI to LI transition indicate KEA3-mediated proton export from the lumen to suppress qE by changing pmf composition in favor of Δψ, particularly in plants from FD_L and DD_F. To confirm this, pmf partitioning was determined from the deconvolved ECS signal 20 s after the transition from HI to LI. No difference could be observed for FD_H plants, but the Δψ component of the pmf was reduced by ~20- 40% in DD_F-*kea3* and significantly by ~44- 55 % in FD_L-*kea3* as compared to the respective WT (Table 1). These results confirm that KEA3-dependent increases in Δψ after HI to LI transitions reflect actual changes in pmf composition.

Together, qE and ECS measurements during light fluctuations corroborated our NPQ results and increased the temporal information on KEA3 and VCCN1 function, revealing that: (i) VCCN1 activity contributes to Δψ dissipation and thereby lumenal acidification and qE activation directly at the onset of HI and (ii) KEA3-mediated proton export from the lumen decreases the lumenal proton concentration and increases Δψ at different time points during light fluctuations in an environment dependent-manner. The results support PFD_{mean} to have an attenuating effect on VCCN1 and promoting on KEA3 function in HI phases. Additionally, we confirm KEA3 to play an important role during qE relaxation after transition from HI to LI by decreasing the ΔpH component of the pmf, but only in FD_L and DD_F. For FD_H at HI, we reveal KEA3-dependent increases in Δψ to precede measurable decreases in qE by ~9 s. This lag in qE suggests that mechanism-intrinsic kinetic constraints delay the response of this mechanism to the lumenal proton concentration at the second time scale.

KEA3 and ATP synthase co-activate in high light.

To obtain further information on the response of the pmf and ATP synthase activity to light fluctuations, we determined the amplitude of the ECS signal at 520 nm as a proxy for light induced pmf (Fig. 4d) and its decay kinetics to derive the trans-thylakoid proton conductivity (g_{H+}, Fig. 4e) during 0.5 s dark intervals that were applied every 10 s throughout the measurement. As expected, pmf increased strongly after transition from LI to HI. After an initial drop that was always observed between the first and second measuring point at HI (at 2 s and 10 s, respectively), growth conditions affected the remaining shape of the pmf response during HI (Fig. 4d). While pmf increased again in FD_L during the subsequent HI treatment, it remained relatively unchanged in DD_F and further decreased in FD_H. For

both flat day conditions, genotype had little effect on pmf. Only *vccn1* had significantly elevated pmf after 46 s of HI in FD_L and 10 s in FD_H, compared to WT. The absence of pmf differences between *kea3* and WT for FD_H and FD_L further confirmed that observed KEA3-dependent changes in Δψ throughout the measurements reflected differences in pmf composition, with KEA3 activity contributing to an increase in Δψ at the expense of ΔpH. No alterations were observed in KEA3 protein content between conditions, emphasizing that the observed KEA3-dependent changes in qE and Δψ were due to differences in KEA3 activation and not KEA3 concentration (Supplemental Fig. 14).

After transition to HI, g_{H+} always decreased at first, and then increased after 10 s in FD_H and DD_F, while continuing to decrease in FD_L until stabilizing after ~30 s at a minimum level (Fig. 4e). Intriguingly, the rise in g_{H+} at HI for FD_H and DD_F coincided with KEA3 activation, as measured by the KEA3-dependent increase in Δψ (Fig. 4c). Lack of KEA3 resulted in reduced g_{H+} in LI after the dark phase, which was independent of growth conditions and additionally led to significant increases in g_{H+} during the entire HI period in DD_F. Loss of *vccn1* resulted in elevated g_{H+} 10 s after the HI-LI shift in FD_L and DD_F, and 10 s after LI-HI shift in DD_F.

Together, our analyses show that lack of ion transport proteins changed the levels of pmf and g_{H+} in plants grown at DD_F with no clear relation to other photosynthetic parameters. For example, lack of either VCCN1 or KEA3 positively affected g_{H+} in HI, while effects on pmf were opposing, positive for *vccn1* and negative for *kea3*. Further work is needed to understand how parameters correlate in DD_F and are influenced by thylakoid ion transport.

KEA3 suppresses zeaxanthin accumulation in a light environment dependent manner.

Based on our analyses, we reasoned that KEA3 deficient plants from DD_F and FD_H should have an increased lumenal proton concentration during at least part of the photoperiod and thus elevated levels of DEPS due to the resulting higher activation of the VDE. Indeed, 6 h into the photoperiod, *kea3* mutants exhibited strongly elevated DEPS both in FD_H and DD_F, but not in FD_L (Fig. 5a). Differences in DEPS between genotypes disappeared after an over-night (ON) dark treatment of DD_F plants. We compared dynamic NPQ of ON-DD_F and >2 h light treated (LT-)DD_F (Supplemental Fig. 15a-b). This analysis revealed that effects of Zx could not be discerned this way, because ON dark treatment strongly suppressed NPQ relaxation, particularly during the first light fluctuation. However, we made two observations: (i) the VCCN1-dependent increase in HI-NPQ requires multiple light fluctuations to

be established. Even after 8 light fluctuations, there was no discernible HI-NPQ difference between ON-*vccn1* and ON-WT (Supplemental Fig. 15c). (ii) NPQ relaxation in *kea3* during the first fluctuation was nearly independent of the length of the dark treatment, while NPQ relaxation of WT and *vccn1* was strongly delayed by the long ON dark treatment (Supplemental Fig. 15d).

Excessive zeaxanthin accumulation delays the response of qE to KEA3-dependent lumenal pH changes.

To further address the question of whether increased levels of Zx influence NPQ relaxation in a KEA3-dependent manner, we employed the *npq2* mutant, which lacks the zeaxanthin epoxidase and thus has a strongly increased VAZ pool with 100% DEPS (Fig. 5b)[21,26]. We grew WT and *kea3* together with *npq2* and *npq2 kea3* double mutants[31] in FD_L and DD_F. In line with our findings from WT and *kea3*, a KEA3-dependent decrease in HI-NPQ in the *npq2* background was only observed in DD_F, but not in FD_L (Fig. 5c), suggesting that KEA3-dependent differences in HI-NPQ between conditions were independent of Zx levels. However, high Zx in *npq2 kea3* further delayed the NPQ decay in the subsequent LI phase when compared to *kea3* alone (Fig. 5d). Because a shift to darkness directly collapsed any NPQ differences between genotypes, these results demonstrate that high Zx slows down the relaxation of qE and not of other more slowly relaxing NPQ components (Supplemental Fig. 16h, j).

Discussion

Dynamic photosynthesis is shaped by light and additional environmental factors.

Our search for acclimatory drivers which exert control on dynamic photosynthesis reveal the mean photon flux density, which plants experience over the day (PFD_{mean}; Intensity: Int in Fig. 6), as a key factor. These results are in line with previous analyses, which demonstrated a strong positive effect of PFD_{mean} on photosynthetic capacity[7,10,11]. Our analyses of dynamic photosynthesis during light fluctuations reveal that high photosynthetic capacity correlates with a reduced need for photoprotective NPQ, avoids the accumulation of longer-term NPQ components and enhances the inhibitory effect that NPQ has on PSII quantum efficiency during short high light phases. The apparent tight dependence of photosynthetic capacity on PFD_{mean} in our study, which includes light fluctuations as a second factor, brings up the intriguing hypothesis that plants have a reliable and precise mechanism to determine PFD_{mean}, even under strong fluctuations in light intensity, and shape plant metabolism accordingly. This mechanism may involve plant photoreceptors and COP1-BBX-Hy5 signaling[36,37].

Fluctuations in light intensity (quantified as PFD_{var}) as part of the growth light regimes had a predominant effect on the levels of VAZ pigments and their de-epoxidation states, which increased strongly with PFD_{var} (Fig. 6, FL: Fluctuating light). Plants grown at high PFD_{var} (DD_F) had a pool of DEPS, which persisted throughout an overnight dark phase (Fig. 5a), proposing fluctuating light as an acclimatory driver independently of light intensity, which controls xanthophyll accumulation and zeaxanthin epoxidase activity.

Our results from polytunnel grown plants demonstrate that other environmental factors besides light affect carbon assimilation capacity and dynamic NPQ (Fig. 6, NE: natural environment). Potential factors are temperature[12,38,39] and light quality[5,6,40], which differed markedly between natural and controlled environments (Supplemental Fig. 1). NE depressed CO_2 assimilation rates and increased the capacity for rapidly reversible NPQ at HI. Both can be explained by the hypothesis that NE acclimation leads to an upregulation of alternative electron transport pathways or sinks that enforce lumen acidification.

Thylakoid ion transport links acclimation with dynamic photosynthesis.

VCCN1 contributes to Δψ dissipation after transition to high light, thereby accelerating lumenal acidification and qE induction (Fig. 6). We show VCCN1 function to be attenuated by increasing PFD_{mean}, with light fluctuations having no apparent effect. VCCN1 was demonstrated to be voltage gated[30]. Our time-resolved ECS measurements revealed LI to HI transitions to induce a Δψ spike, which was more pronounced when compared to overall Δψ levels in FD_L-plants than in the other two conditions (Fig. 4g-i). We hypothesize that photosynthetic capacity, which increases with PFD_{mean}, attenuates the initial spike in Δψ after transition to HI, thereby decreasing VCCN1 activation and function. Another possible explanation is the upregulation of so far unknown other Δψ-dissipating thylakoid channels in response to increasing PFD_{mean}.

KEA3 exports protons from the lumen and thereby decreases qE, while retaining pmf (Fig. 6). Our results uncover that KEA3 contributes to qE suppression in high light, a function which correlates strongly with PFD_{mean}, suggesting a dependence on photosynthetic capacity (Fig. 2). By time-resolved analysis of the membrane potential, we found KEA3 activation to coincide with an increase in ATP synthase activity. The observed rise in ATP synthesis can be explained by the release of metabolic backpressure when the CBB cycle becomes more active after some time in HI, consuming ATP and

301 releasing inorganic phosphate as well as ADP. Further support for a metabolic activation of KEA3
302 comes from comparing KEA3-dependent NPQ relaxation after HI-LI shifts between plants exposed to
303 different lengths of dark treatments. The strong inactivation of downstream metabolism by an ON dark
304 treatment was accompanied by very small effects of KEA3 on NPQ, suggesting that KEA3 was largely
305 inactive. Previously, it was shown that KEA3 inactivation at HI of low-light grown plants requires its C-
306 terminus. This regulatory part of KEA3 carries a KTN-domain with a nucleotide binding site[32,33].
307 NAD(P)H and ATP were found to be regulatory ligands of other regulatory KTN domains[41-43]. Thus,
308 metabolic regulation may occur allosterically by NADP(H) or alternatively ATP, as suggested by the
309 potential simultaneous regulation of KEA3 and ATP synthase activity.

310 Our analyses uncover the *kea3* high NPQ phenotype during LI relaxation to be enhanced by PFD_{var}.
311 We show KEA3 to partly counteract PFD_{var}-induced Zx accumulation, suggesting that high Zx in *kea3*
312 further delays NPQ relaxation, already hindered by the absence of KEA3-mediated proton export from
313 the lumen. Our analyses of *npq2* and *npq2 kea3* double mutants confirm that high levels of Zx
314 exacerbate the *kea3*-dependent lag in qE relaxation. These results reinforce the hypothesis that Zx has
315 a kinetic effect on qE dynamics[23,27], and propose that high Zx counteracts a rapid response of qE to the
316 lumenal proton concentration.

317 In summary, our results demonstrate that rapid responses of photosynthesis are strongly affected by
318 long-term acclimation to the growth environment. This discovery mandates future crop improvement
319 strategies, which pursue the acceleration of photosynthetic responses, to consider acclimation effects
320 on target regulator functions.

321 **Material & Methods**

322 **Plant material & growth**

323 *Arabidopsis thaliana* plants were grown in 6 cm pots on horticultural substrate (MPG mixture from
324 Stender, Schermbeck, Germany with 1 g/l Osmocote start) in phytochambers (BBC York, Mannheim,
325 Germany) with a 12 h light period during the day and temperatures/ relative humidity set to 20 °C/ 60
326 % in the light and 16 °C/ 75 % in the dark, under six different light conditions from seed to mature
327 rosette. Three flat day (FD) conditions were applied, with 90 (low, FD_L), 250 (medium, FD_M) or 900 µmol
328 photons m^{-2} s^{-1} (high, FD_H; Fig. 1a). Additionally, three dynamic day (DD) conditions were applied with
329 varying light intensities over the day period (Fig. 1a): Fluctuating DD (DD_F) had 144 repetitions of the

same light fluctuation (4 min 90, 1 min 900 µmol photons m^{-2} s^{-1}), sinusoidal DD (DD_S) had a gradual increase and decrease in light intensity peaking at midday (maximum: 960 µmol photons m^{-2} s^{-1}) and sinusoidal fluctuating DD (DD_{SF}) was DD_S with added fluctuations in light intensity, occurring at random intervals and frequency and averaging 250 µmol photons m^{-2} s^{-1} to allow comparison with FD_M and DD_F. Lighting in FD and DD_F was provided by white, blue and red LEDs (Roschwege, Greifenstein, Germany, blue: 450 nm, red: 660 nm), with both blue and red light combined accounting for 40 % of the light intensity and white light for 60 %. Light intensity at the rosette level was adjusted by changing set output of the LEDs or varying the distance between plants and LEDs. Lighting in DD_S and DD_{SF} conditions was provided by white LEDs only to facilitate programming of the chamber with random fluctuations. For natural day (ND) experiments, plants were grown in 13 cm pots in a polytunnel at the MPI of Molecular Plant Physiology (coordinates: 52° 24' 55.44'' N; 12° 58' 7.464'' E). After three weeks of pre-cultivation in a phytotron (120 µmol photons m^{-2} s^{-1}, climate conditions as described above), plants were grown in the polytunnel from 21.03. to 28.03.2019 (ND_1) or from 04.04. to 14.04.2019 (ND_2). Measurements were done on day 7 and 8 after transfer for ND_1 and day 8 and 9 for ND_2. Measurements were performed on mature plants (FD_L: 5-6 weeks, FD_M: 4-5 weeks FD_H: 3-4 weeks, DD_S: 3-4 weeks, DD_F: 5-6 weeks, DD_{SF}: 4-5 weeks) 1-2 weeks before bolting. The analyses were performed on Arabidopsis wild-type Columbia-0 (WT) and on T-DNA insertion mutants in the WT background as previously published (*vccn1-1*: Salk 103612; *vccn1-2*: Gabi-Kat 796C09, *kea3-1*: Gabi-Kat 170G09; *kea3-2*: Sail 556_E12, *npq2*: Salk_059469, *npq2 kea3*[13,30,31]). Experiments including the *npq2* and *npq2 kea3-1* mutants were performed on plants grown at elevated humidity under a dome. To determine biomass accumulation, rosettes were harvested at indicated times after sowing and dry weight was determined after oven-drying (75 °C, 7 d). PFD_{mean} represents the average light intensity and PFD_{var} the sum of light intensity changes over the day, both in µmol photons m^{-2} s^{-1}.

Chlorophyll *a* fluorescence & absorbance measurements

For Chl *a* fluorescence analyses, the MAXI IMAGING-PAM (Walz, Effeltrich, Germany) or an integrated diode emitter array spectrophotometer/ fluorometer (IDEAspec)[44] were used on whole rosettes or a section of one fully expanded leaf, respectively. Saturation light pulses of 0.8 / 0.5 s, respectively, were applied after 30 min dark treatment to determine Fm, during illumination with actinic light for Fm', and during dark relaxation for Fm''. Non-photochemical quenching (NPQ) was calculated as (Fm − Fm′)/Fm′, Φ_{PSII} as (Fm′ − F')/Fm′, Fv/Fm as (Fm – F0)/Fm, NPQ_f as a measure for qE as (Fm″ – Fm′)/Fm′ and

360 NPQ_s after 5 min of darkness as (Fm − Fm″)/Fm″ (reviewed by Baker 2008[45]). Absorbance changes at
361 6 different wavelengths (475, 488, 505, 520, 535, 545 nm), were measured near-simultaneously on the
362 IDEAspec[44] separated by 1 ms intervals and recorded every 30 ms. Measuring light was supplied by
363 red LEDs (655 nm, bandpass ~ 20 nm), as described in Hall et al., 2021[44]. The absorbance changes
364 were deconvoluted at each time point by least squares fitting to four simultaneous linear equations,
365 describing the contributions to absorbance combinations of the four components ECS, qE, zeaxanthin
366 and drift to absorbance changes at the six wavelengths described above:

367 $$\Delta A_\lambda = ECS \cdot \epsilon_{\lambda,ECS} + qE \cdot \epsilon_{\lambda,qE} + Zx \cdot \epsilon_{\lambda,Zx} + drift \cdot \epsilon_{\lambda,drift}$$

368 Where λ represents the measurement wavelength, ECS, qE, Zx and drift represent the extents of the
369 four contributing components, and $\epsilon_{\lambda,ECS}, \epsilon_{\lambda,qE}, \epsilon_{\lambda,Zx}$ and $\epsilon_{\lambda,drift}$ represent the normalized relative
370 extinction coefficients for the given components at wavelength λ, as summarized in Supplemental
371 Table_Fig4c. The normalized, effective extinction coefficients for ECS were determined by measuring
372 absorbance changes following a 1 ms subsaturating light pulse and a subsequent 10 ms dark relaxation
373 phase, which at this time scale predominantly reflect the ECS signal[46,47]. Relative extinction coefficients
374 for the qE- and Zx-related signals were approximated using the approach of Bilger et al., 1989[48]. The
375 spectrum for the drift component was determined by measuring absorbance changes in dark acclimated
376 leaves over a time scale of about 1-3 minutes, and thus reflects slow changes in leaf optical properties
377 (e.g., caused by leaf movements, light scattering changes, chloroplast movements etc.) that are likely
378 not related to photochemistry.

379 Four iterations of the following light pattern were applied during the measurement: 4 min of 90, 1 min
380 of 900, 20 s of 90 µmol photons m^{-2} s^{-1} followed by 30 s darkness. During each iteration, ECS traces
381 were drift corrected using the last 15 s of the dark phase and qE traces using 10 s of the LI just before
382 the HI transition. Δψ and ΔpH were calculated from the multiphasic ECS kinetics during the 30 s dark
383 interval[34,35]. Total light-induced pmf (ECS_t) and trans-thylakoid proton conductivity of ATP synthase
384 (g_{H+}) were calculated from dark interval relaxation kinetics at 520 nm[49]. Plants were exposed to the
385 same light fluctuations as described above and every 10 s, a 500 ms dark interval was applied. The
386 first 60 ms of the dark interval were used to determine g_{H^+} as the rate constant of a first order exponential
387 decay.

388

Quantification of photosynthetic complexes and proteins

For immunoblot analysis, total protein was extracted from liquid nitrogen-frozen plant rosettes, supplemented with lysing matrix D (MP Biomedicals)[50]. In detail, the Fastprep 24 tissue homogenizer (MP Biomedicals) was set to 6.5 s^{-1} and tissue was disrupted for 1 min. 200 µl protein extraction buffer (200 mM Tris, pH 6.8, 8 % SDS (w/v), 40 % glycerol and 200 mM DTT) was added to 20 mg of ground leaf tissue. Samples were heated at 65 °C for 10 min and proteins were separated on SDS-PAGE, blotted onto nitrocellulose, visualized with Ponceau Red (0.1 % Ponceau S (w/v) in 5% (v/v) acetic acid, used for Rubisco quantification) and detected with antibodies specific for KEA3[31], Lhcb3, PsbD, PetA, PsaA, AtpB and Actin (Agrisera, diluted according to manufacturer's instructions). The signal intensities of specific proteins from individual blots were determined via ImageJ, and first normalized on the signal intensity of FD_M. Then, normalized values were corrected for loading by FD_M-normalized actin signals of the same blot. Raw intensities can be found in Supplemental Table_SFig3_SFig4b.

For MS analysis, thylakoid isolation was performed 2 h into the photoperiod by using whole plant rosettes[31]. Proteins were extracted and digested[51]. Sample processing and LC-MS/MS data acquisition (see also Supplemental Table_SFig4b_1) settings and raw data processing were performed as described[33,52] with the following adjustments: Peptides were purified using SDP-RPS stage tips[53] prior to LC-MS analysis. MaxQuant 1.6.17.0[54] was used with default settings. Match between runs and intensity-based absolute quantification (iBAQ) were additionally enabled[33,52]. iBAQ data was used for quantification to compensate for contaminators during thylakoid preparation. Photosynthetic complexes were used for normalization[4] (for details see Supplemental Table_SFig4b_1).

Pigment extraction & analysis

Arabidopsis rosettes were harvested and plunged into liquid N_2. Harvest was performed in the phytochambers 6 h into the photoperiod (in low light phase for DD_F plants). Pigments were extracted either from 20 mg of ground leaf powder or from thylakoid membranes, isolated as described in the previous section, corresponding to 20 µg of chlorophyll, by addition of 100 % acetone on ice and in the dark. The pigment extract was filtrated through a PTFE filter (0.2 µm pore size) and filtrates were analyzed according to Färber et al., 1997[55].

Gas exchange measurements

Gas exchange was measured in 2 s intervals either on whole plants, using the LI-COR 6400 gas exchange system (Li-Cor Biosciences, Lincoln, Nebraska, USA; Flow rate: 500 µmol s^{-1}, CO_2 concentration: 400 µmol mol^{-1}, humidity: 60 %) coupled to the Imaging PAM (Walz GmbH, Germany saturation pulse for 0.8 s at intensity setting 5, every 1 min) or on single leaves, using the GFS-3000 open gas exchange system with the LED array unit 3056-FL (Walz GmbH, Effeltrich, Germany; Flow: 600 µmol s^{-1}, CO_2 concentration: 400 µmol mol^{-1}, humidity: 60 %) on the youngest fully developed leaf in a 3 x 1 cm cuvette. Prior to each measurement, plants were dark-acclimated for 30 min, inserted into the cuvette and then exposed to 10 min of 900, then 10 min of 90 µmol m^{-2} s^{-1} and 5 min of darkness. CO_2 assimilation rate was normalized on the leaf area inserted into the cuvette. Net assimilation rates (A_n) and dark respiration (R_d) were averaged over the final 30 s of the light phases or subsequent dark phase, respectively. Gross assimilation rate (A_g) at high irradiance was determined as the sum of HI-A_n and respiration in the dark (A_g= HI-A_n + R_d).

Statistics & Clustering

Normality distribution and equal variance were confirmed by one- or two-way ANOVA and a Tukey multiple comparison test was performed in SigmaPlot 14.5 (Systat Software GMBH, Erkrath, Germany) or Rstudio (version 3.5.3). If normality and/ or equal variance test failed, an ANOVA on ranks was performed and subsequently the Student-Newman-Keuls method when analyzing the same number of biological replicates or Dunn's test when numbers varied between groups. One-way ANCOVA was performed in SAS 9.4 (SAS Institute, Cary, NC, USA) using growth conditions as class variable and PFD_{mean} and PFD_{var} as covariates. Multiple regression analysis was performed by using either SAS or SigmaPlot. Correlation analysis was performed using Python or SigmaPlot, employing either Pearson's or Spearman's rank correlation for linear or monotonic relationships, respectively. K-mean clustering of the fast NPQ response was performed on log_2 transformed, normalized NPQ (genotype/WT) in Python.

Data availability

Raw proteomics data were deposited via JPOST (Moriya et al., 2019) under the following identifiers JPST001271. The data is available under the following link for reviewers and will be made publicly available upon publication. URL: https://repository.jpostdb.org/preview/165610471160fff0bf9c33e, access key: 3887

Code availability

The script used for generating the DD_{SF} light treatment in the phytotron is available online (https://github.com/EliasKaiser/Fluctuations/blob/main/190614_Lightfleck_program.R).

References

1 Kaiser, E., Morales, A. & Harbinson, J. Fluctuating Light Takes Crop Photosynthesis on a Rollercoaster Ride *Plant Physiology* **176**, 977-989 (2017).

2 Bailey, S., Horton, P. & Walters, R. G. Acclimation of Arabidopsis thaliana to the light environment: the relationship between photosynthetic function and chloroplast composition. *Planta* **218** (2004).

3 Bailey, S., Walters, R. G., Jansson, S. & Horton, P. Acclimation of Arabidopsis thaliana to the light environment: the existence of separate low light and high light responses. *Planta* **213**, 794-801 (2001).

4 Flannery, S. E. *et al.* Developmental acclimation of the thylakoid proteome to light intensity in Arabidopsis. *The Plant Journal* **105**, 223-244 (2021).

5 Walters, R. G. & Horton, P. Acclimation of Arabidopsis thaliana to the light environment: Changes in composition of the photosynthetic apparatus. *Planta* **195**, 248-256 (1994).

6 Walters, R. G. & Horton, P. Acclimation of Arabidopsis thaliana to the light environment: regulation of chloroplast composition. *Planta* **197**, 475-481 (1995).

7 Athanasiou, K., Dyson, B. C., Webster, R. E. & Johnson, G. N. Dynamic Acclimation of Photosynthesis Increases Plant Fitness in Changing Environments. *Plant Physiology* **152**, 366-373 (2009).

8 Schumann, T., Paul, S., Melzer, M., Dörmann, P. & Jahns, P. Plant Growth under Natural Light Conditions Provides Highly Flexible Short-Term Acclimation Properties toward High Light Stress. *Front Plant Sci* **8**, 681 (2017).

9 Mishra, Y. *et al.* Arabidopsis plants grown in the field and climate chambers significantly differ in leaf morphology and photosystem components. *BMC Plant Biology* **12**, 6 (2012).

10 Vialet-Chabrand, S., Matthews, J. S., Simkin, A. J., Raines, C. A. & Lawson, T. Importance of Fluctuations in Light on Plant Photosynthetic Acclimation. *Plant Physiology* **173**, 2163-2179 (2017).

11 Alter, P., Dreissen, A., Luo, F.-L. & Matsubara, S. Acclimatory responses of Arabidopsis to fluctuating light environment: comparison of different sunfleck regimes and accessions. *Photosynthesis Research* **113**, 221-237 (2012).

12 Pescheck, F. & Bilger, W. High impact of seasonal temperature changes on acclimation of photoprotection and radiation-induced damage in field grown Arabidopsis thaliana. *Plant Physiology and Biochemistry* **134**, 129-136 (2019).

13 Duan, Z. *et al.* A bestrophin-like protein modulates the proton motive force across the thylakoid membrane in Arabidopsis. *J Integr Plant Biol* **58**, 848-858 (2016).

14 Külheim, C., Ågren, J. & Jansson, S. Rapid Regulation of Light Harvesting and Plant Fitness in the Field. **297**, 91-93 (2002).

15 Pribil, M. *et al.* Fine-Tuning of Photosynthesis Requires CURVATURE THYLAKOID1-Mediated Thylakoid Plasticity. *Plant Physiology* **176**, 2351-2364 (2018).

16 Demmig-Adams, B. *et al.* Using chlorophyll fluorescence to assess the fraction of absorbed light allocated to thermal dissipation of excess excitation. *Physiologia Plantarum* **98**, 253-264 (1996).

17 Johnson, M. P. *et al.* Photoprotective energy dissipation involves the reorganization of photosystem II light-harvesting complexes in the grana membranes of spinach chloroplasts. *The Plant Cell* **23**, 1468-1479 (2011).

18 Briantais, J. M., Vernotte, C., Picaud, M. & Krause, G. H. A quantitative study of the slow decline of chlorophyll a fluorescence in isolated chloroplasts. *Biochimica et Biophysica Acta* **548**, 128-138 (1979).

19 Li, X. P. *et al.* Regulation of photosynthetic light harvesting involves intrathylakoid lumen pH sensing by the PsbS protein. *The Journal of Biological Chemistry* **279**, 22866-22874 (2004).

20 Li, X.-P. *et al.* A pigment-binding protein essential for regulation of photosynthetic light harvesting. *Nature* **403**, 391-395 (2000).

21 Niyogi, K. K. Arabidopsis mutants define a central role for the xanthophyll cycle in the regulation of photosynthetic energy conversion. *The Plant Cell* **10**, 1121-1134 (1998).

22 Arnoux, P., Morosinotto, T., Saga, G., Bassi, R. & Pignol, D. A structural basis for the pH-dependent xanthophyll cycle in Arabidopsis thaliana. *The Plant Cell* **21**, 2036-2044 (2009).

23 Tutkus, M. *et al.* Single-molecule microscopy studies of LHCII enriched in Vio or Zea. *Biochim Biophys Acta Bioenerg* **1860**, 499-507 (2019).

24 Xu, P., Tian, L., Kloz, M. & Croce, R. Molecular insights into Zeaxanthin-dependent quenching in higher plants. *Sci Rep* **5**, 13679 (2015).

25 Holt, N. E. *et al.* Carotenoid cation formation and the regulation of photosynthetic light harvesting. *Science* **307**, 433-436 (2005).

26 Johnson, M. P., Pérez-Bueno, M. L., Zia, A., Horton, P. & Ruban, A. V. The zeaxanthin-independent and zeaxanthin-dependent qE components of nonphotochemical quenching involve common conformational changes within the photosystem II antenna in Arabidopsis. *Plant physiology* **149** (2009).

27 Sacharz, J., Giovagnetti, V., Ungerer, P., Mastroianni, G. & Ruban, A. V. The xanthophyll cycle affects reversible interactions between PsbS and light-harvesting complex II to control non-photochemical quenching. *Nature Plants* **3**, 16225 (2017).

28 Mitchell, P. Chemiosmotic coupling in oxidative and photosynthetic phosphorylation. *Biol Rev Camb Philos Soc* **41**, 445-502 (1966).

29 Kramer, D. M., Cruz, J. A. & Kanazawa, A. Balancing the central roles of the thylakoid proton gradient. *Trends Plant Sci* **8**, 27-32 (2003).

30 Herdean, A. *et al.* A voltage-dependent chloride channel fine-tunes photosynthesis in plants. *Nature Communications* **7**, 11654 (2016).

31 Armbruster, U. *et al.* Ion antiport accelerates photosynthetic acclimation in fluctuating light environments. *Nature Communications* **5**, 5439 (2014).

32 Armbruster, U. *et al.* Regulation and Levels of the Thylakoid K+/H+ Antiporter KEA3 Shape the Dynamic Response of Photosynthesis in Fluctuating Light. *Plant Cell Physiology* **57**, 1557-1567 (2016).

33 Uflewski, M. *et al.* Functional characterization of proton antiport regulation in the thylakoid membrane. *Plant Physiology*, doi:10.1093/plphys/kiab135 (2021).

34 Cruz, J. A., Sacksteder, C. A., Kanazawa, A. & Kramer, D. M. Contribution of electric field (Δy) to steady-state transthylakoid proton motive force (pmf) *in vitro* and *in vivo*. control of pmf parsing into Delta psi and Delta pH by ionic strength. *Biochemistry* **40**, 1226-1237 (2001).

35 Takizawa, K., Cruz, J. A., Kanazawa, A. & Kramer, D. M. The thylakoid proton motive force in vivo. Quantitative, non-invasive probes, energetics, and regulatory consequences of light-induced pmf. *Biochimica et Biophysica Acta* **1767**, 1233-1244 (2007).

36 Alvarez-Fernandez, R. *et al.* Time series transcriptomics reveals a BBX32-directed control of acclimation to high light in mature Arabidopsis leaves. *The Plant Journal* doi:10.1111/tpj.15384 (2021).

37 Walters, R. G., Rogers, J. J., Shephard, F. & Horton, P. Acclimation of Arabidopsis thaliana to the light environment: the role of photoreceptors. *Planta* **209**, 517-527 (1999).

38 Herrmann, H. A., Schwartz, J. M. & Johnson, G. N. From empirical to theoretical models of light response curves - linking photosynthetic and metabolic acclimation. *Photosynthesis Research* **145**, 5-14 (2020).

39 Vile, D. *et al.* Arabidopsis growth under prolonged high temperature and water deficit: independent or interactive effects? **35**, 702-718 (2012).

40 Wagner, R., Dietzel, L., Bräutigam, K., Fischer, W. & Pfannschmidt, T. The long-term response to fluctuating light quality is an important and distinct light acclimation mechanism that supports survival of Arabidopsis thaliana under low light conditions. *Planta* **228**, 573-587 (2008).

41 Cao, Y. *et al.* Gating of the TrkH ion channel by its associated RCK protein TrkA. *Nature* **496**, 317-322 (2013).

42 Kröning, N. *et al.* ATP binding to the KTN/RCK subunit KtrA from the K+ -uptake system KtrAB of Vibrio alginolyticus: its role in the formation of the KtrAB complex and its requirement in vivo. *The Journal of Biological Chemistry* **282**, 14018-14027 (2007).

43 Roosild, T. P., Miller, S., Booth, I. R. & Choe, S. A mechanism of regulating transmembrane potassium flux through a ligand-mediated conformational switch. *Cell* **109**, 781-791 (2002).

44 Hall, C. C. *et al.* Photosynthetic Measurements with the Idea Spec: an Integrated Diode Emitter Array Spectrophotometer/Fluorometer, in *Photosynthesis Research for Food, Fuel and the Future* 184-188, doi.org/10.1007/978-3-642-32034-7_38 (2013).

45 Baker, N. R. Chlorophyll fluorescence: a probe of photosynthesis in vivo. *Annual Review of Plant Biology* **59**, 89-113 (2008).
46 Bailleul, B., Cardol, P., Breyton, C. & Finazzi, G. Electrochromism: a useful probe to study algal photosynthesis. *Photosynthesis Research* **106**, 179-189 (2010).
47 Kramer, D. M. & Sacksteder, C. A. A diffused-optics flash kinetic spectrophotometer (DOFS) for measurements of absorbance changes in intact plants in the steady-state. *Photosynthesis Research* **56,** 103-112 (1998).
48 Bilger, W., Björkman, O. & Thayer, S. S. Light-induced spectral absorbance changes in relation to photosynthesis and the epoxidation state of xanthophyll cycle components in cotton leaves. *Plant Physiology* **91**, 542-551542 (1989).
49 Kanazawa, A. & Kramer, D. M. In vivo modulation of nonphotochemical exciton quenching (NPQ) by regulation of the chloroplast ATP synthase. *Proc Natl Acad Sci U S A* **99**, 12789-12794 (2002).
50 Armbruster, U. *et al.* Regulation and Levels of the Thylakoid K+/H+ Antiporter KEA3 Shape the Dynamic Response of Photosynthesis in Fluctuating Light. *Plant & Cell Physiology*, doi:10.1093/pcp/pcw085 (2016).
51 Morgan, M. J. *et al.* Decrease in manganese superoxide dismutase leads to reduced root growth and affects tricarboxylic acid cycle flux and mitochondrial redox homeostasis. *Plant Physiology* **147**, 101-114 (2008).
52 Lassowskat, I. *et al.* Dimethyl-Labeling-Based Quantification of the Lysine Acetylome and Proteome of Plants. *Methods in Molecular Biology (Clifton, N.J.)* **1653**, 65-81 (2017).
53 Kulak, N. A., Pichler, G., Paron, I., Nagaraj, N. & Mann, M. Minimal, encapsulated proteomic-sample processing applied to copy-number estimation in eukaryotic cells. *Nature Methods* **11**, 319-324 (2014).
54 Cox, J. & Mann, M. MaxQuant enables high peptide identification rates, individualized p.p.b.-range mass accuracies and proteome-wide protein quantification. *Nature Biotechnology* **26,** 1367-1372 (2008).
55 Färber, A., Young, A. J., Ruban, A. V., Horton, P. & Jahns, P. Dynamics of Xanthophyll-Cycle Activity in Different Antenna Subcomplexes in the Photosynthetic Membranes of Higher Plants (The Relationship between Zeaxanthin Conversion and Nonphotochemical Fluorescence Quenching). *Plant Physiology* **115**, 1609-1618 (1997).

Acknowledgements

We recognize P. Pieloch for excellent technical support and thank M.A. Schöttler for valuable discussions and help with the phytotrons. We acknowledge help with plant cultivation by the MPI-MP greenteam. U.A. and D.M.K. are supported by the 3rd call ERA-CAPS grant (NSF IOS-1847193 and DFG AR 808/4-1). U.A. received funding from the DFG (AR 808/5-1) and the Max Planck Society.

Author contributions

UA and TvB designed the study. TvB performed most experimental work with help from JR and KS and supervision from VG during the initial stage of the study. KüK prepared thylakoids, which were analyzed by JE and IF. PJ performed pigment analyses, EK set up the phytotron for random light fluctuations, KaK helped with the polytunnel experiments and performed statistical analyses. JAC and DMK designed and supervised the absorption spectroscopy approach, which were interpreted by UA, TvB, and DMK. DDS helped analyzing spectroscopy data. UA and TvB wrote the manuscript with contributions and input from all authors.

Competing interests

The authors declare no competing interests.

Additional information

Supplementary information (PDF)

Supplementary Tables (Excel spreadsheet)

Figures/ Tables:

Table 1: The Δψ component of pmf during qE relaxation.

The Δψ component of pmf was determined at 20 s after the third HI to LI shift. Average of n = 4-7 ± SD is provided. Statistically significant differences to WT, as determined by one-way ANOVA and Tukey multiple comparison test, are indicated by asterisks (* $p < 0.05$).

Growth Condition	WT	*kea3-1*	*kea3-2*	*vccn1-1*	*vccn1-2*
FD_L	84.6 ± 12.9	38.1 ± 3.3*	47.6 ± 2.0*	78.7 ± 5.1	80.1 ± 7.8
FD_H	86.3 ± 7.2	85.3 ± 4.7	83.4 ± 5.2	80.1 ± 7.9	86.8 ± 4.1
DD_F	100 ± 0.0	60.5 ± 14.8	79.5 ± 12.7	99.3 ±1.4	100 ± 0.0

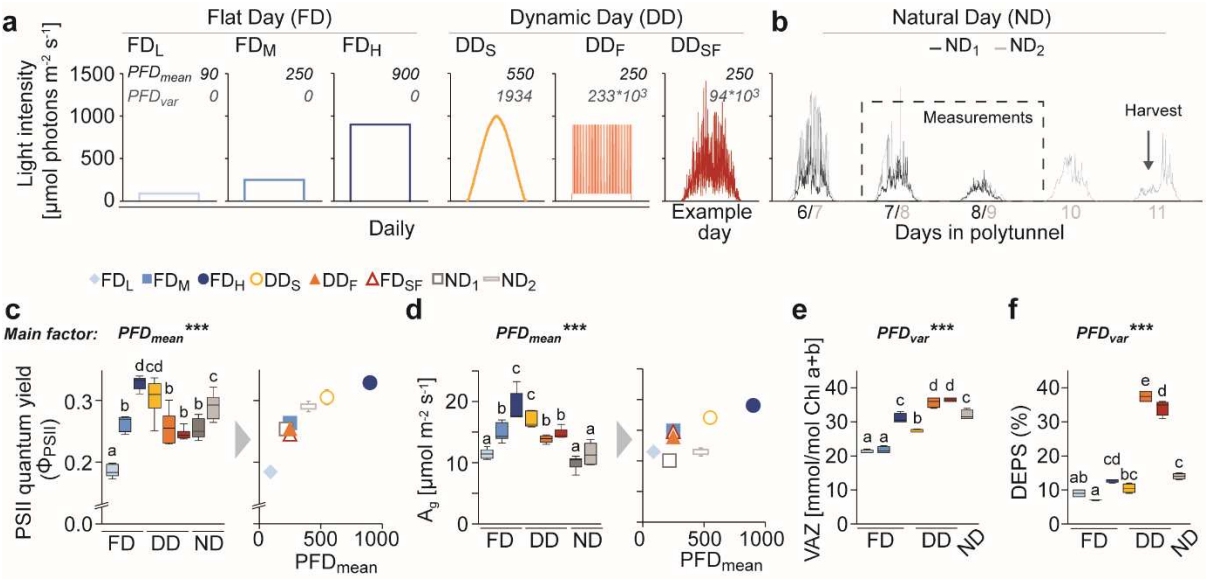

Fig. 1: Environmental acclimation adjusts steady state photosynthesis and thylakoid pigment composition.

a-b, Plants were grown in 12 h/ 12 h light/ dark cycles under constant growth light (flat day, FD) at indicated intensities (low, FD_L; medium, FD_M; high, FD_H), dynamic growth light (dynamic day, DD) with varying degrees of light fluctuations (sinusoidal, DD_S; step-wise fluctuating, DD_F; sinusoidal with random light fluctuations, $DD_{SF;}$ a) or natural growth conditions in a foil green house (natural day, ND_1; ND_2; b). **a**, Average and variable photon flux densities (PFD_{mean} and PFD_{var}, respectively) are displayed. **b**, daily PFD_{mean} and PFD_{var} for b can be found in Supplemental Fig. 1h-i and Supplemental Table_Fig1a-b_SFig1. **c-d,** PSII quantum efficiency (Φ_{PSII}; c, left panel) at 700 µmol photons m^{-2} s^{-1} and gross assimilation rate (A_g, d, left panel) at 900 µmol photons m^{-2} s^{-1} increase with PFD_{mean} as the main factor, and plotted against PFD_{mean} (c-d, right panels). PFD_{mean} for ND was determined as average of the 3 days before the measurement. Averages of n = 5-7 ± SE are shown. **e-f,** Levels of photoprotective xanthophylls (VAZ, sum of violaxanthin, antheraxanthin, zeaxanthin; e) and their de-epoxidation state (DEPS, f) are positively influenced by PFD_{var} as the main factor. Averages of n = 4 ± SE are shown. **c-f**, An ANCOVA was used to determine effects of PFD_{mean} and PFD_{var} on parameters. The main factor is indicated on top of the panels with *** denoting p< 0.0001. Statistical analyses can be found in Supplemental Table_Fig1c, Supplemental Table_Fig1d_SFig2c and Supplemental Table_Fig1e-f.

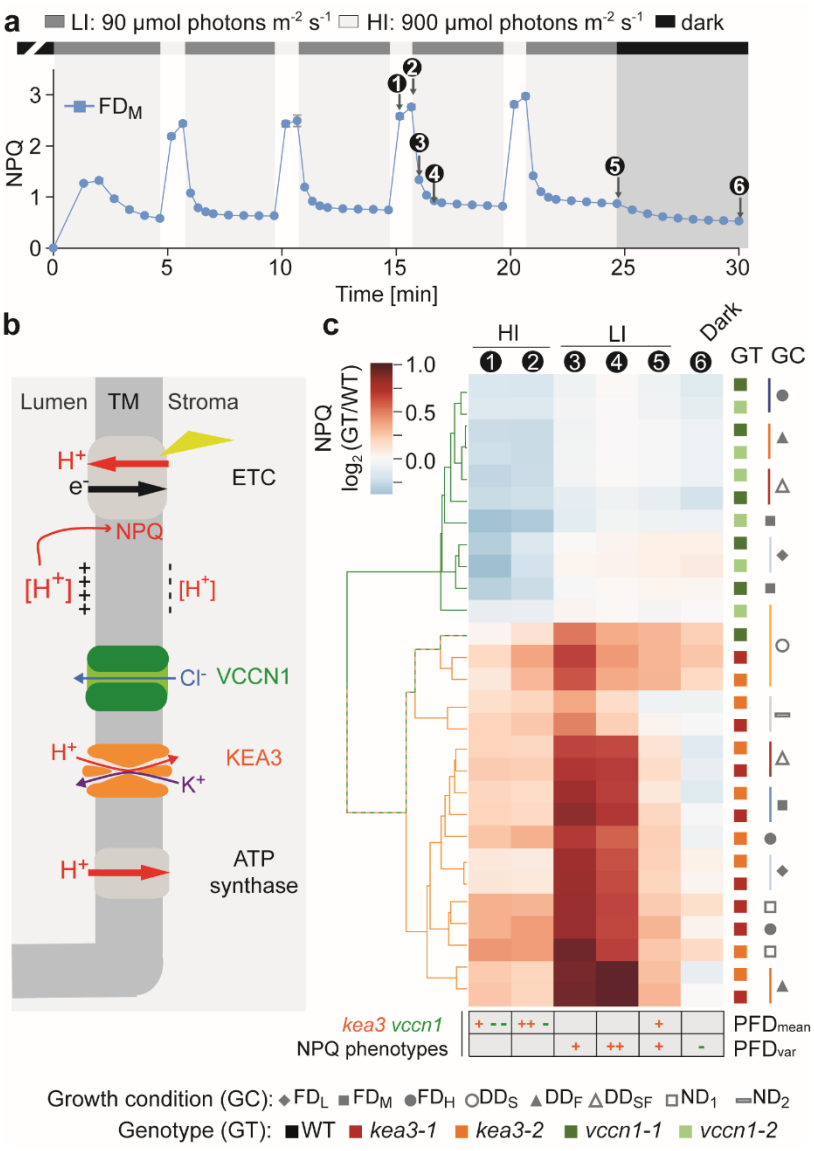

Fig. 2: Light acclimation interacts with the function of thylakoid ion transport proteins.

a, NPQ traces in fluctuating light (high irradiance, HI; low irradiance, LI) of dark-acclimated WT plants grown under FD_M. Averages of n = 5-7 ± SE are shown. Comparative analyses of NPQ between all different growth environments (FD_L, FD_M, FD_H, DD_S, DD_F, DD_{SF}, ND_1, ND_2; shown in Fig. 1a-b) and statistical analyses can be found in Supplemental Fig. 5 and Supplemental Table_SFig5a. **b**, Scheme of the electron transport chain (ETC), the ATP synthase, the VCCN1 chloride channel and the KEA3 proton K^+ antiporter located in the thylakoid membrane (TM). **c,** Clustered heatmap of log_2 transformed genotype (GT)/ WT NPQ ratios of two *kea3* and *vccn1* alleles from the different light environments (growth light, GL) at the 6 different time points indicated in a. Multiple regression analysis was performed on the GT/WT NPQ ratios using average and variable photon flux densities (PFD_{mean} and PFD_{var}, respectively) as covariates. Significant effects on the NPQ genotype compared to WT are displayed below the heatmap (*vccn1*, green; *kea3*, red; +, increasing; -, decreasing with +/- $p < 0.05$ and ++/-- $p<0.001$). Statistical analyses can be found in Supplemental Table_Fig2c_SFig8.

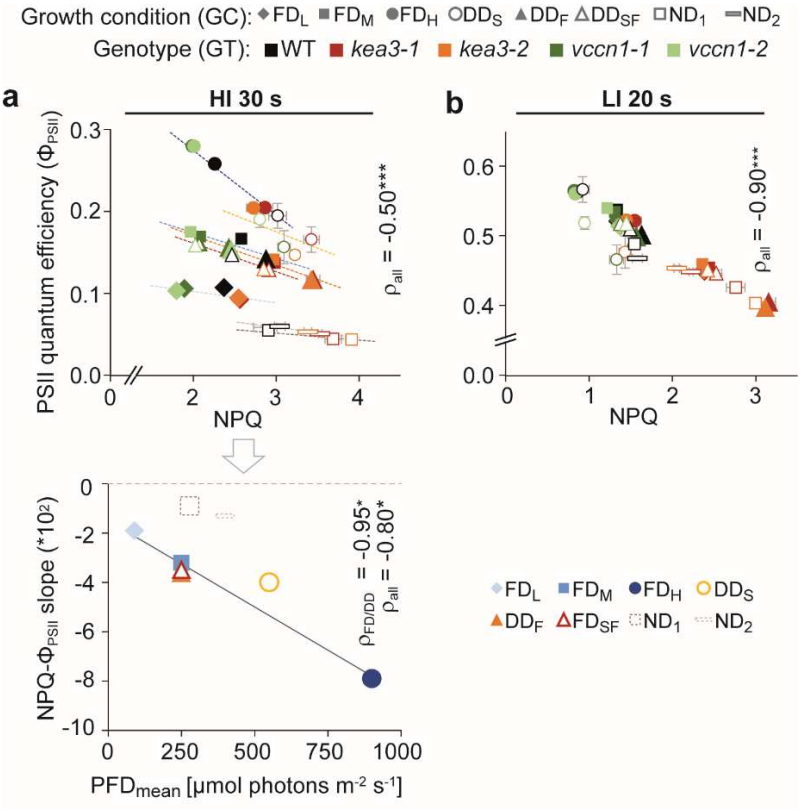

Fig. 3: Growth light intensity determines the effect of thylakoid ion transport on photosynthetic efficiency.

a-b, Φ_{PSII} plotted against NPQ of WT, *kea3* and *vccn1* lines from 8 different growth conditions (FD_L, FD_M, FD_H, DD_S, DD_F, DD_{SF}, ND_1, ND_2; Fig. 1a-b) at 30 s after transfer from LI to HI (HI 30 s; a, upper panel) and 20 s after transfer from HI to LI (LI 20 s, b) during the third light fluctuation as shown in Fig. 2a. Colored dashed lines indicate environment specific slopes according to the figure's color scale of conditions (a, upper panel), showing a strong correlation with average photon flux density (PFD_{mean}; a, lower panel). Averages of n = 3-7 ± SE are shown. Pearson correlation coefficient ρ is given for all points (ρ_{all}) or phytotron grown plants only ($\rho_{FD/DD}$; a, lower panel) and asterisks indicate significant correlation with * $p<0.05$ and *** $p<0.0001$. Environmental specific slopes for all time points and for different groups of points with corresponding ρ can be found in Supplemental Table_Fig3_SFig9.

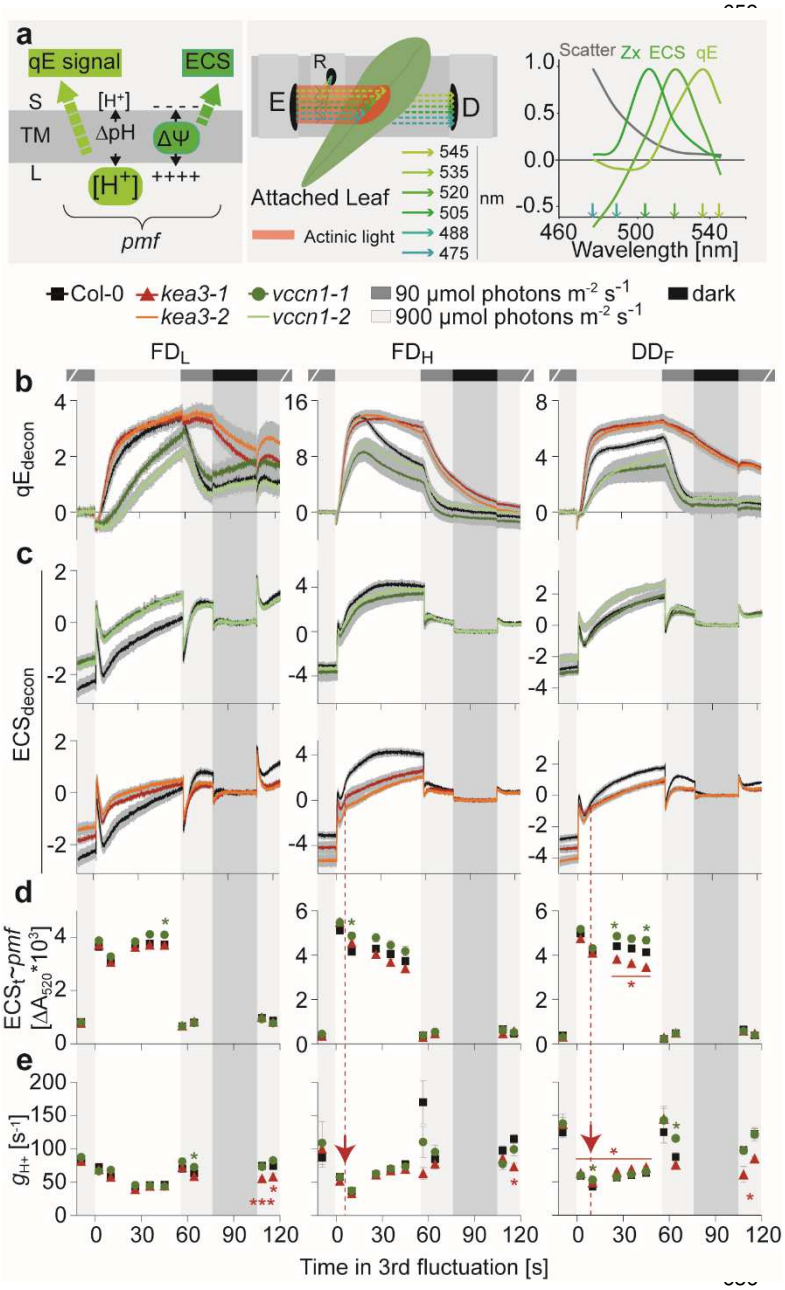

Fig. 4: A newly modified spectroscopy approach reveals light-environmental effects on the function of thylakoid ion transport proteins.

a, Both pmf components can be assessed by simultaneous measurements of energy-dependent quenching (qE) that responds to the lumenal proton concentration and therefore changes in ΔpH and the ECS signal which approximates changes in membrane potential (Δψ). S − stroma; L − lumen; TM − thylakoid membrane; pmf − proton motive force (left). Spectroscopic set-up with emitter (E), detector (D) and reference detector (R) to measure absorption of attached mature leaves near simultaneously at 6 wavelengths (middle). Absorption spectra of components used for deconvolution (right). **b-c,** Changes in the qE (b) and ECS (c) signals of WT and two mutant alleles each of *kea3* and *vccn1* grown in FD_L, FD_H and DD_F during the third light fluctuation. Averages of n = 4-7 ± SE are shown. qE and ECS traces of the entire fluctuating light treatment can be found in Supplemental Tables _Fig4d-f and _Fig4g-l. **d-e,** ECS_t (d) and g_{H+} (e) determined from short dark pulses applied to the same fluctuating light set-up as in b-c of WT, *kea3-1* and *vccn1-1* plants grown in FD_L, FD_H and DD_F. The third and fourth light fluctuations were averaged with n = 4-6 ± SE. Asterisks in the corresponding color indicate significant differences as compared to WT, determined by one-way ANOVA and subsequent Tukey multiple comparison test with * $p<0.5$ and *** $p<0.0001$. Red arrows indicate time points of KEA3 activation as estimated from c. Please note that in d-e, time resolution is much lower as compared to c and thus there is no information on the actual g_{H+} minimum, which may be before the second measuring point.

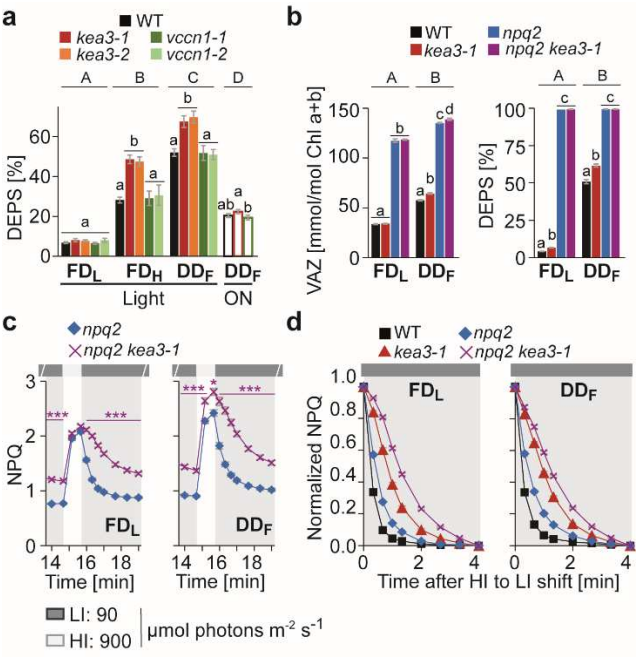

Fig. 5: KEA3 suppresses Zx in the light, with high Zx accumulation delaying the response of NPQ to changes in lumen pH.

a, The de-epoxidation state (DEPS) of the pool of the xanthophyll cycle pigments violaxanthin, antheraxanthin and zeaxanthin (VAZ) was determined at 6 h into the light period from WT, and two mutant alleles each of *kea3* and *vccn1* grown in FD_L, FD_H or DD_F and of DD_F plants after an overnight (ON) dark treatment. A one-way ANOVA with Tukey multiple comparison test revealed significant differences between all conditions as indicated by the different capital letters. Lowercase letters indicate significant differences between genotypes within a single treatment. Averages of n = 4-5 ± SE are shown. **b,** VAZ pool (left) and its de-epoxidation state (DEPS, right) of FD_L and DD_F grown WT, *kea3-1*, *npq2* and *npq2 kea3-1*. Averages of n = 5 ± SE are shown. Different capital letters above the graph and lowercase letters indicate significant differences between growth conditions or genotypes within a given condition, respectively, as determined via two-way ANOVA and subsequent Student-Newman-Keuls test. **c-d,** NPQ traces (c) or NPQ relaxation kinetics (d) during the third fluctuation of plants grown in FD_L (left) or DD_F (right). Averages of n = 6 ± SE are shown. Full NPQ and Φ_{PSII} traces can be found in Supplemental Fig. 16h-k. **c**, Asterisks in the corresponding color indicate significant differences between *npq2 kea3-1* and *npq2*, determined by one-way ANOVA and subsequent Tukey multiple comparison test with * p<0.5 and *** p<0.0001.

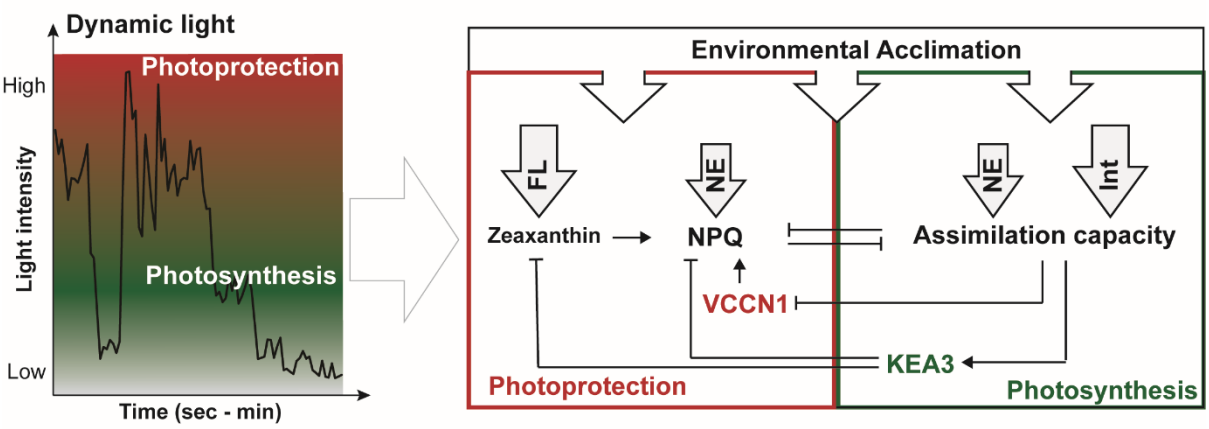

Figure 6: Model of effects by environmental acclimation on dynamic photosynthesis and connection with thylakoid ion transport proteins.

In dynamic light environments, the switch between photoprotection and efficient photosynthesis is governed by environmental acclimation. The right scheme highlights the identified acclimation factors (FL: fluctuating light; NE: natural environment; Int: light intensity as light grey, black lined arrows) and summarizes their effects on photosynthesis and photoprotection. FL and Int had strong positive effects on either zeaxanthin accumulation or assimilation capacity, respectively. NE positively affected NPQ and negatively assimilation capacity. Black arrows indicate activating or inhibitory effects between the photosynthetic components and thylakoid ion transport proteins. VCCN1 promotes photoprotection by increasing NPQ. KEA3 promotes photosynthesis by downregulating zeaxanthin and NPQ. Both VCCN1 and KEA3 link assimilation capacity with photoprotection. At low assimilation capacity, VCCN1 is on and KEA3 is off during HI phases, while the reverse occurs at high assimilation capacity. KEA3 counteracts zeaxanthin accumulation in FL to suppress NPQ (i.e. accelerate NPQ relaxation in LI).

Supplementary Files

This is a list of supplementary files associated with this preprint. Click to download.

- 210929SupplementaryinformationTB.pdf
- 210928SupplementalTables.xlsx